LA-UR -82-1586

Conf-820470--1

MASTER

Los Alamos National Laboratory is operated by the University of California for the United States Department of Energy under contract W-7405-ENG-36.

TITLE: NEUTRON-ANTINEUTRON EXPERIMENT AT LOS ALAMOS OMEGA WEST REACTOR

AUTHOR(S): H. L. An P-DO

SUBMITTED TO: Neutron-Antineutron Oscillation Workshop
Cambridge, MA, April 30 - May 1, 1982

Los Alamos Los Alamos National Laboratory
Los Alamos, New Mexico 87545

FORM NO 836 R4
ST NO 2629 5/81

NEUTRON-ANTINEUTRON EXPERIMENT AT LOS ALAMOS OMEGA WEST REACTOR

H. L. Anderson+

Los Alamos National Laboratory*

General Arrangement

Figure 1 shows an overview of the experimental arrangement. The Omega West Reactor lies at the bottom of a canyon. We use a drift tube 50 meters long. That puts the detector and the building that houses it inside the canyon wall. The wall will have to be cut out somewhat for the purpose. The canyon setting provides a useful amount of shielding against cosmic rays.

Figure 2 is a close-up view showing the reactor core. Graphite stringers are removable from the front end of the thermal column close to reactor core. By taking the thermalized neutrons off in a direction tangential to the core, fast neutrons and direct gamma rays from the core are greatly reduced in number. Within the reactor building the drift tube is 24 inches in diameter surrounded by steel plates to keep the radiation at tolerable levels within the building.

Figure 3 shows the drift tube and detector building in more detail. Note the beam stop beyond the detector and note the overburden above the building for additional cosmic ray shielding.

Figure 4 is an elevation view of the detector building showing detector location and a crane for handling the detector elements.

---

*Work performed under the auspices of the U.S.D.O.E.

+Talk presented at "Informal Workshop on Neutron-Antineutron Oscillations" Harvard University, April 30-May 1, 1982

Capture Gamma Rays

All sources of thermal neutrons are accompanied by a substantial flux of capture gamma rays. In the case of the Omega West Reactor we used a 3-dimensional Monte Carlo transport code[1] to calculate the number of thermal neutrons and capture gammas emerging from the thermal neutron channel TC-1S. The calculation was normalized to the neutron fluxes actually measured in the thermal column. The neutron energy distribution is taken to be Maxwellian at 350° K. Within the angular range $0.92 \leq \cos\theta \leq 1.00$, the numbers of neutrons and gamma rays exiting from the channel were found to be

$$\text{Neutron flux} \qquad 5.5 \times 10^{12}\ s^{-1}$$

$$\text{Gamma flux} \qquad 5.0 \times 10^{11}\ s^{-1}\ .$$

The gamma flux from the reactor is about 10% of the neutron flux. The gammas have an energy distribution given in the table below.

TABLE I

Energy distribution of gamma rays
from thermal neutron channel TC-1S.

Gamma Energy MeV	Fraction
0.0-0.2	0.13
0.2-0.5	0.19
0.5-1.0	0.17
1.0-2.0	0.07
2.0-5.0	0.17
5.0-10.0	0.27

Such a large γ/n ratio would overwhelm our detector unless precautions were taken to reduce the number entering the sensitive regions of the detector by a large factor. Accordingly, in common with other

arrangements except Grenoble, we have adopted a cylindrical arrangement in which the detector surrounds a thin target.

The target is thin enough to transmit most of the neutrons and gamma rays in the beam without intereaction. It is thick enough to intercept the antineutrons in the beam and cause, with high probability, their annihilation.

To keep the gamma rays from the reactor from entering the sensitive region of the detector, an elaborate baffle system has been designed as shown in the foreshortened view of Figure 5.

The baffles are made of lead faced with ^{6}LiF. The production of capture gammas which are absorbed by ^{6}Li is reduced by a factor of 5×10^{-5}. The lead absorbs gamma rays from the reactor which might otherwise enter the sensitive region of the detector.

Gamma rays which traverse the target are stopped further downstream by a beam stop, lined with ^{6}LiF. The beam stop is far enough down stream to keep the number of backward moving gammas that might enter the sensitive region of the detector at tolerable levels.

The total intensity of gammas (and neutrons) in the beam is reduced by extending the length of the drift tube to 50 meters. This is to be compared to 20-30 meters in other designs. The number of $n \cdot \bar{n}$ conversions is proportional to the square of the drift length, ℓ^2, which compensates the ℓ^{-2} loss in neutron flux.

We carried out a Monte Carlo calculation of the number of neutrons crossing the target and of the number of gamma rays entering the sensitive volume of the detector. This is a 3-dimensional transport code available at Los Alamos.[1] The calculation included the effect of

adding a 1.2-cm Pb liner on the inside surface of the detector. The results are given in Table 2.

TABLE 2

Neutron and gamma fluxes at the detector.

Neutron flux at the target:		3.3×10^{11} s^{-1}
For $\tau = 10^7$ seconds, $n \rightarrow \bar{n}$ conversions:		0.25/day
Capture gammas into the detector:	without Pb:	7.4×10^6 s^{-1}
	with 1.2 cm Pb:	3.6×10^6 s^{-1}
Reactor gammas into the detector:	without Pb:	6.5×10^7 s^{-1}
	with 1.2 cm Pb:	8.7×10^6 s^{-1}

	Gammas from neutron beam Fraction		Gammas from reactor Fraction	
Energy MeV	No Pb	1.2 cm Pb	No Pb	1.2 cm Pb
0.0-0.2	0.05	0.00	0.23	0.00
0.2-0.5	0.09	0.04	0.33	0.16
0.5-1.0	0.20	0.19	0.20	0.32
1.0-2.0	0.03	0.07	0.11	0.28
2.0-5.0	0.34	0.38	0.12	0.24
5.0-10.0	0.29	0.32	0.01	0.00

The results for reactor gammas into the detector refer to a calculation with the neutrons from the reactor turned off. Capture gammas into the detector refers to the calculation made with the reactor neutrons on and the reactor gammas off.

Our design has reduced the ratio γ's into detector/neutrons into target to 4×10^{-5}. The absolute number of γ's entering the detector, 1.2×10^7 s^{-1}, is easily managed. Moreover, we have designed the

detector to be virtually insensitive to low energy γ's, provided only that pile-up effects are not serious.

Liquid Scintillators

Our detector is made entirely of liquid scintillator modules following closely the design of the University of Pennsylvania group, K. Lande et al., for their Homestake Mine proton decay experiment.[2]

This design has several features that meet the needs of an anti-neutron annihilation detector:

1. Good time resoltuion, 3 ns FWHM.
2. Long attenuation length, 8 m.
3. Large fraction of energy deposition made visible.
4. Low cost.

In Figures 6 and 7 we reproduce the tables in the Homestake Mine proton decay experiment which give the characteristics of the liquid scintillator modules we propose to use in our detector.

Detector

In the course of a 200-day run some 10^{10} cosmic rays will traverse the detector. It must be able to distinguish unambiguously even one annihilation event if that occurs during this time.

We rely heavily on time of flight to tell annihilation events that come from the target from cosmic rays that come from the outside. A cross-sectional view of the detector is shown in Figure 8. Immediately surrounding the drift tube is a square array of liquid scintillator counters each 6" x 6" x 26' long, the A counters. There follows a 4' gap and then a square array of liquid scintillators 12" x 12" x 26'

long, copies of the Homestake Mine scintillator design. The innermost layer of these is designated the B counters, the next C, and so on until the outermost eighth layer which is designated the I counters.

Each scintillator is viewed by two 5" photomultipliers with hemisperical cathodes and have been shown to have a time resolution of 3 ns FWHM. A time-of-flight measurement between counters A and B will be able to show, in most cases, that particles are moving from inside out and not from outside in. With the direction of motion of the annihilation pions established the scintillator array as a whole measures the energy deposited by each. The detector is thick enough to stop most of the π° induced electromagnetic showers (6 radiation lengths). Low energy pions will range out by ionization loss. Higher energy pions will interact with the nuclei of the scintillator liquid (3 nuclear absorption lengths).

In liquid scintillator the charged pions have a high probability of interacting with a nucleus, producing a nuclear disintegration The liquid scintillator makes visible the nuclear disintegration energy and so records not only the kinetic energy of the pion but its rest energy as well. This feature is lost in lead glass Cerenkov counters and in lead scintillator sandwich calorimeters. For pions that decay before they have a chance to have a nuclear interaction, the neutrinos in the chain $\pi \rightarrow \mu\nu$ $\mu \rightarrow e\bar{\nu}\nu$ are not seen by any detector. The energy of these neutrinos is not a large fraction of the total released.

With the addition of end sections, as shown in Figure 9, the acceptance of the detector for particles from the target is 95%. In summary our detector has the following characteristics:

1. Time of flight over 4 foot gap tells direction of particle motion.

2. Reconstructs vertex at the target (spatial resolution 60 cm FWHM).

3. Verifies time of flight from target (time resolution 3 ns FWHM).

4. Acceptance is 95%; visible energy is 84%.

5. Measures energy and momentum of each particle.

6. Checks energy and momentum conservation (allowance must be made for Fermi motion and nuclear excitation induced by the annihilation in the target nucleus).

An important feature of the liquid scintillator modules we use is their insensitivity to capture gamma rays. The liquid scintillation counters are thick, either 15 cm or 30 cm. In the 15-cm thickness the dE/dx ionization loss is 27 MeV, much higher than the 7-MeV maximum from capture gammas. Thus, setting a threshold somewhat above 7 MeV renders the scintillator insensitive to capture gammas, at least insofar as a coincidence is required between the two PM tubes viewing the scintillator at each end. Of course, pile-up could cause serious problems. That is why we have gone to so much trouble to bring the gamma flux down to manageable levels.

Since the response of the scintillator modules is not uniform along the length, it is possible for a capture gamma ray near one end of the scintillator to produce a large pulse in the nearby photomultiplier that is above threshold. This could produce an incorrect mean time reading. At our levels of γ flux this will occur only a small fraction of the time.

Annihilation Cross Section

We need to know the annihilation cross section to ensure that all the antineutrons that strike the target will annihilate. There are no direct measurements with low energy antineutrons. However, a reasonable estimate can be made from what is known about anitproton interactions. In particular, the low energy behavior of antiprotons can be obtained from measurements on the x rays of antiprotonic atoms. Once the antiproton is captured in an atomic orbit of high quantum number n, it proceeds to make transitions to more tightly bound energy levels with successively smaller n. At sufficiently small n, e.g., the $4 \rightarrow 3$ transition in C or the $5 \rightarrow 4$ transition in S, the strong interaction with the nucleus affects the transition in measurable ways. There is a shift in the energy from its Dirac value, there is a broadening in the line width, and there is a reduction in the intensity of the line because nuclear absorption competes with the emission of radiation in the transition. Using a single optical potential, the data from some 20 transitions over a wide range of elements have been fitted successfully.[3] The resulting scattering length turned out to be,

$$\bar{a} = (1.53 \pm 0.27) + i(2.50 \pm 0.25) \text{ fm} \quad .$$

Similar results have been obtained by Roberson et al.,[4] and by Poth et al.[5] The absorption cross section is obtained from the following formula based on the optical theorem,

$$\sigma_a = 2\lambda \mathrm{Im}(\quad) \quad ,$$

where $\lambda = h/p$ is the deBroglie wavelength. For antineutrons with a

velocity of 2200 m s^{-1}, λ = 2Å and $\sigma_a = 8 \times 10^{-21}$ cm^2. The cross section is per nucleus. There is no A dependence.

This result can be checked by comparing it to an extrapolation of the 1/v behavior of the $\bar{p}d$ cross section at higher energies.

Measurements of $\bar{p}d$ by Kalogeropoulos et al.[6] in the range 0.26 to 0.47 GeV/c give the following annihilation cross sections in the low velocity limit,

$$\sigma(\bar{p}p) = \frac{37}{\beta} \text{ mb} \quad , \quad \text{and} \quad \sigma(\bar{p}n) = \frac{28}{\beta} \text{ mb} \quad ,$$

where β is the velocity in units of c. For v = 2200 m s^{-1}, $\sigma_a \cong$ 4.5×10^{-21} cm^2.

At low velocities the deBroglie wavelength of the antiproton is much greater than nucleon dimensions and it is not correct to add the cross sections as is the case for the deuteron at higher energies. Nevertheless, the high energy results are in rough agreement with the p-atom result.

With a cross section of 8000 b, a 5-mil Be target is overkill. However, if the cross section were 4 times less the absorption would slip to 96%. We would want to use a thicker target if the cross section were any smaller than this. Clearly, it will be important to measure the cross section more directly for a proper interpretation of the experiment.

Magnetic Shielding

Figure 10 shows the importance of magnetic shielding. The curve is calculated for a drift length of 10 meters and a neutron velocity distribution which is Maxwellian at 400° K. The conversion is suppressed appreciably, more than 10%, above 8×10^{-3} gauss. What counts

is $\int B \cdot d\ell$. Thus, for a 50-meter drift length the average field has to be below 1.6×10^{-3} gauss. This is not easy to do. It requires a multilayer mu metal shield plus coils for demagnetizing the mu metal and for bucking out any residual fields that remain.

Vacuum Requirements

It is not hard to satisfy the requirement of no nuclear collision in the drift tube. The mean free path in air at NTP corresponding to a cross section of 8×10^{-21} cm^2 is 2 cm. Even a vacuum pressure of less than 10^{-3} mm of Hg would already suffice to reduce the probability of an annihilation collision in 50 meters to less than 1%. At the other extreme, avoiding even molecular collisions that might inhibit the growth of the antineutron amplitude, we consider 10^{-16} cm^2 as an upper limit to the cross section. This is also the unitarity limit for a velocity of 2200 m s^{-1}. This would require a vacuum of 10^{-7} torr. On the other hand, we have not been able to identify a mechanism with such a high cross section which would be different for neutron than for antineutron. We conclude that a vacuum of 10^{-4} torr should be more than adequate for our purposes.

Cosmic-Ray Background

The Omega West Reactor is at an altitude of 2100 meters. Its geomagnetic latitude is near 40° N. The atmospheric depth is about 800 g/cm^2. The total cosmic ray intensity is

$$I_T(\text{at } 40^\circ \text{ N}, 800 \text{ g cm}^{-2}) = 2.1 \times 10^{-2} \text{ cm}^{-2} \text{ s}^{-1} \text{ sr}^{-1} ,$$

enough to produce a pulse rate of 500 s^{-1} in each of the 30 cm x 800 cm

counters in the detector.

A 10-cm thick layer of lead above the top of the detector will remove the soft component. What remains are mainly muons, which are the principal constituents of the cosmic rays, about 3/4 of the total. With 1000 gm/cm^2 of passive shielding above the detector, the muon intensity will be reduced somewhat to 40% of its incident value. Thus, we expect,

$$I_\mu(\text{at } 40^\circ \text{ N, } 1800 \text{ g cm}^{-2}) = 6 \times 10^{-3} \text{ cm}^{-2} \text{ s}^{-1} \text{ sr}^{-1} \quad .$$

The effective solid angle is about 1 sr, the area subtended by the inner array of counters is 1.7×10^5 cm^2. Thus, the rate of single muons traversing the detector will be about 1000 per second. We quote this rate to emphasize how high the rejection ratio must be to bring the trigger rate down to manageable values. The trigger is insensitive to single muons. It requires a minimum of 3 tracks, all coming from the center of the detector. This part of the trigger requirement, however, could be met by a chance coincidence of two such muons if one muon is suitably delayed within the 15-ns gate used to determine that the tracks are outgoing. A veto is important here.

A muon produced shower is another possibility. However, since the radiation length of muons is 4×10^4 times greater than it is for electrons, the production of muon induced electromagnetic showers is at the 10^{-4} level. Muon induced hadronic showers are at about the same level but become significant only for high energy muons of several GeV or more. The veto suppresses the response to entering muons by a factor of 10^2, while the time-of-flight requirements of the trigger

provide a further reduction by a factor of 10^2. The anticipated rate is, thus, 10^{-5} s^{-1}, about 1/day. These are comfortable trigger rates. They allow plenty of time for off line analysis to rule them out on the basis of the additional pulse height and spatial information that then becomes available. In quoting these figures we are not unmindful that the detector is vulnerable to cosmic rays that enter horizontally along the drift tube. Here the Omega West site offers the advantage of being set in the bottom of a canyon in a setting that provides an appreciable amount of natural shielding against horizontal cosmic rays.

Cosmic Ray Neutrons

The veto is not effective against neutral particles that enter the detector unaccompanied by charged particles. One such possibility is a muon induced large angle bremsstrahlung in the material above the detector, in which the muon misses the detector but the gamma ray enters unaccompanied by an electronic component. The cosmic ray neutrons are more dangerous. They can enter the detector without producing a pulse in the outer layers. Inside the detector they interact with high probability and could produce a multiparticle hadronic shower capable of setting the trigger. Although the trigger is specially designed to discriminate against such events, we suppose it will fail to do so in about 1% of the cases.

At GeV energies we may take the neutron-proton ratio to be close to 1 and estimate the neutron intensity from the following formula[7] for the differential vertical intensity of the protons:

$$J_p(W,h) = 1.0 \times 10^{-3}\, he^{-h/l_*}(W + a)^{-\alpha-1} \quad ,$$

with L = 125 g cm^{-2}, α = 1.8, a = 0.9 GeV, h is the thickness of the atmosphere in g cm^{-2}, and W the neutron kinetic energy in GeV. For neutrons above 2 GeV at sea level (h = 1000 g cm^{-2}) integration of the above expression gives,

$$J_n = 1.5 \times 10^{-5} \text{ cm}^{-2} \text{ s}^{-1} \text{ sr}^{-1} \quad .$$

The shielding above the detector is important here. With 1000 g cm^{-2} of shielding h = 1.8×10^3 g cm^{-2} and the integrated intensity for neutrons above 1 GeV is found to be

$$J_n(>2.2 \text{ GeV}, 1800 \text{ g cm}^{-2}) = 3 \times 10^{-8} \text{ cm}^{-2} \text{ s}^{-1} \text{ sr}^{-1} \quad .$$

To produce a trigger the neutron induced shower would have to be in the vicinity of the target, within an effective area of about 5×10^4 cm^2. Using a trigger rejection ratio of 100 for such events we anticipate a trigger rate of 1.5×10^{-5} s^{-1}, about 1 per day. This is an entirely manageable trigger rate. It gives ample opportunity for the off-line analysis to reject these events.

Most cosmic ray background events will have pulses from the entering particles that come earlier than those that activate the trigger. We propose to identify these in an inspector circuit and veto events that show pulses earlier than those that give the trigger. This should reduce cosmic ray background events to even lower levels.

Trigger

Good events originate at the target and have all particles moving outward. In cosmic ray events the particles are moving from the outside in. We use time of flight to tell the direction of particle.

However, although the first part of the track of a cosmic ray particle is moving from outside in, it moves from inside out after it traverses the inside region. In a cosmic ray shower, we could have several tracks moving from inside out. Thus, it is not sufficient to have a delayed coincidence showing 3 or more particles moving from inside out.

We have to provide a veto whenever there is a particle from the outside moving in. Referring to Figure 11, we identify the successive rings of counters as A,B,C,...I. The separation $\underline{AB}$ is 4.5 feet. The minimum time of flight between A and B is 4.5 ns, more if the track is oblique instead of perpendicular to the axis of the detector. The flight time difference between A and B for an outward moving particle compared to one going the other way is at least 9 ns, a time easily resolved by our counters with a σ = 1.5 ns.

For the purposes of a trigger we divide the A counter into 8 sections as shown in Figure 11. We denote by B_i the counters in B (includes the end counters) associated with the i^{th} octant for particles that originate in the target. We form the coincidence,

$$Q_i = A_i^d \cdot B_i \quad ,$$

where the superscript d means that the coincidence is delayed to correspond to outgoing particles. The trigger is formed by requiring $N \geq 3$ coincidences,

$$T = (Q_i \cdot Q_j \cdot Q_k \cdot .....) \cdot \bar{V} \quad .$$

This scheme is an adaptation of the one proposed by Ellis.[8] The cosmic ray veto is on straight through tracks as signaled by a delayed

coincidence in any pair of B sections that includes an A counter in its trajectory. We call this veto V_1.

As an alternate veto, V_2, we use an inspector circuit that looks for C·B coincidence coming earlier than the ≥3 coincidence among the A sections that have satisfied the trigger requirement. In our arrangement, we could have an improvement in efficiency by increasing the number of sections and reducing the probability that two of the tracks would be in the same octant.

Included in the veto, to improve its efficiency for charged particles, is a delayed coincidence using the outer counters I_1,

$$V_3 = \sum_i I_i^d \cdot A_i \quad .$$

The time of flight between I and A is typically 12 ns, so this veto is less affected by time jitter effects. The vetoes V_1 and V_2 are effective against neutron induced showers. The complete veto is

$$V = V_1 + V_2 + V_3 \quad .$$

Certain cosmic ray shower events could give a false trigger due to jitter in the pulse of one of the upper B counters through which a vertical cosmic ray particle has passed. We have to ask how effective is the time-of-flight differential of 9.6 ns in differentiating an incoming from an outgoing vertical track. The time resolution of the counters has been measured. Its rms value is $\sigma = 1.5$ ns. To recognize an outgoing track the pulse from the A counter has to be delayed by 4.5 ns and made about 15 ns long. To make the A·B coincidence occur with high probability for an outgoing track the B pulse

has to be $3\sigma = 4.5$ ns wide. If the track is incoming we have to ask what is the probability that the B pulse will deviate by an amount δ from its mean value, enough to cause a coincidence with the delayed A signal. Assuming a gaussian response, the probability is given by

$$P(\delta/\sigma) = \frac{1}{\sqrt{2\pi}} \int_{\delta/\sigma}^{\infty} e^{-t^2/2}\, dt \quad .$$

For the worst case, vertical cosmic ray tracks, $\delta/\sigma = 3.4$, $P(3.4) = 3.4 \times 10^{-4}$. This number has to be multiplied by the number of vertical tracks in the shower. While this may be a satisfactory suppression factor, it is vulnerable in practice to a slippage in the δ/σ ratio. Thus, with $\delta/\sigma = 3$, $P(3) = 1.4 \times 10^{-3}$, which is 4 times less effective. For this reason it is worth while incorporating a separate veto for the vertical cosmic rays.

The trigger efficiency for a three-fold coincidence depends on the conversion probability of the π° gamma rays which traverse the A counters. Moreover, an inefficiency results if one of the charged pions from the annihilation suffers a nucleon interaction before it reaches the B counter. Using the known branching ratio for the different annihilation modes we have estimated a trigger efficiency of 60% in our arrangement.

In Table 3 we present a summary of the characteristics and sensitivities of n-$\bar{n}$ conversion experiments running, under construction, and proposed.

Table $\tilde{\Lambda}$ $n \to \bar{n}$ Experiment

$\nu = (t/\tau)^2 \, \phi T_c$

$t = \ell/v \quad T = 1.73 \times 10^7$ s (200 d) $\quad \tau = 10^7$ s

Experiment	drift length ℓ m	drift time $t=\ell/v$ s	neutron flux ϕ ns^{-1}	Figure of Merit ϕt^2 ns	detection efficiency ϵ	no. events for $T=10^9$ s ν	sensitivity at "zero" background τ_{min} 90% CL s
Grenoble II	6	3×10^{-3}	10^9	9×10^5	0.35	0.054	1.5×10^6
Pavia	16	7×10^{-3}	3×10^{11}	1.4×10^7	0.50	1.3	0.7×10^6
Oak Ridge	20	8×10^{-3}	4×10^{13}	3×10^9	0.50	215.	1×10^8
(with Bi-D_2O moderator)			6×10^{12}	4×10^8	0.50	29.	4×10^7
LAMPF							
(probable)	30	1.4×10^{-2}	2×10^{12}	4×10^8	0.50	34.	4×10^7
(possible)			4×10^{12}	8×10^8	0.50	68.	5×10^7
Omega West	50	2.3×10^{-2}	3×10^{11}	1.5×10^8	0.50	13.	2×10^7
Grenoble III	35	9×10^{-2}	10^{12}	8×10^9	0.50	700.	1.7×10^8

References

1. "MCMP--A General Monte Carlo Code for Neutron and Photon Transport", Los Alamos Report LA-7396-M, Revised Nov. 1979.

2. Proposal to the USDOE to construct the Homestake Mine Tracking Spectrometer, A Deep 1400-Ton Nucleon Decay Detector. The University of Pennsylvania, K. Lande et al. Sept. 1981.

3. C. J. Batty, "Exotic Atoms: A Review", Rutherford and Appleton Laboratories, RL-80-094 (1980).

4. P. Roberson, T. King, et al., Phys. Rev. C16, 1945 (1977).

5. H. Poth, G. Backenstoss, et al., Nucl. Phy. A294, 435 (1978).

6. T. Kalogeropoulos and C. S. Tzanakos, Phys. Rev. D22, 2285 (1980).

7. S. Hayakawa, Cosmic Ray Physics, p. 336, John Wiley & Sons, New York (1969).

8. R. J. Ellis et al., "A Neutron Oscillation Experiment at LAMPF", LAMPF Proposal #647.

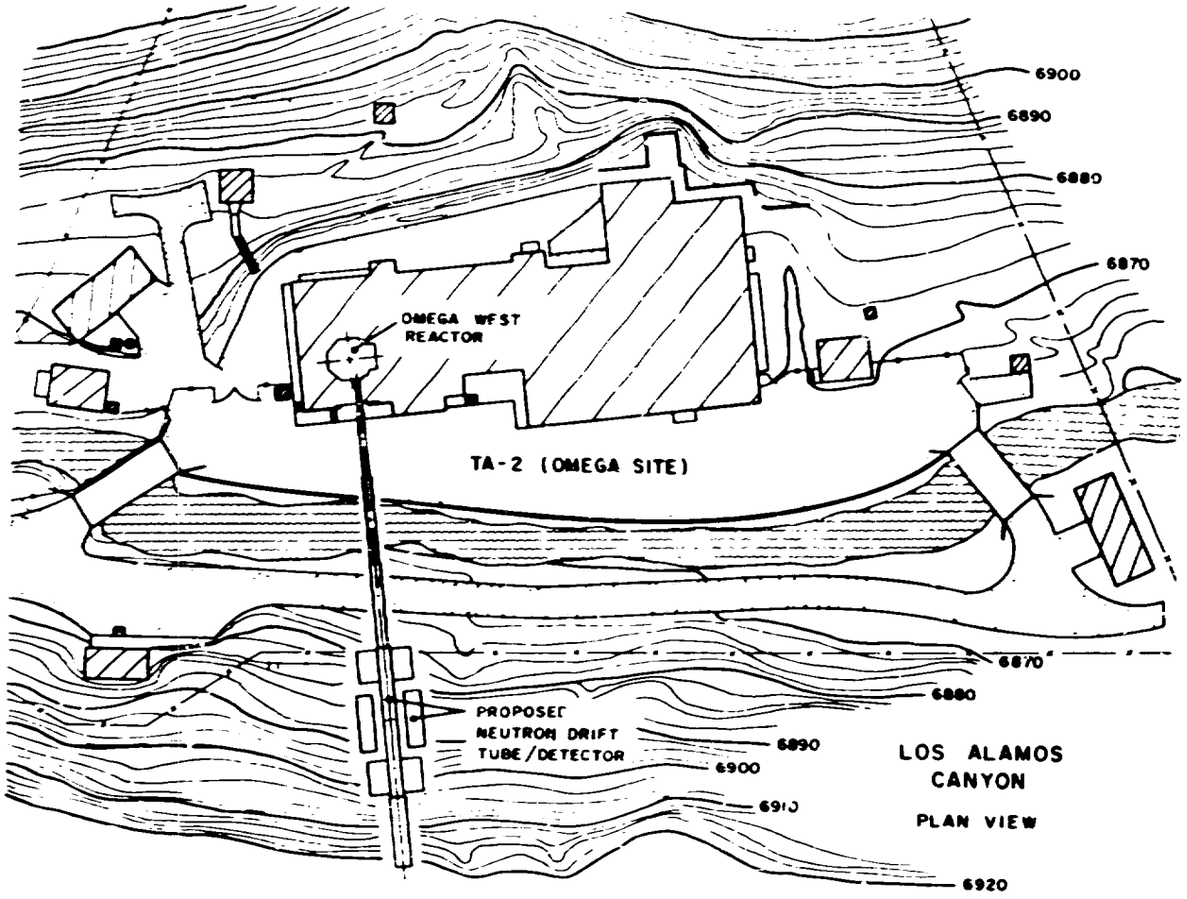

Figure 1. Overview of the neutron-antineutron experiment in the canyon at the site of the Omega West Reactor.

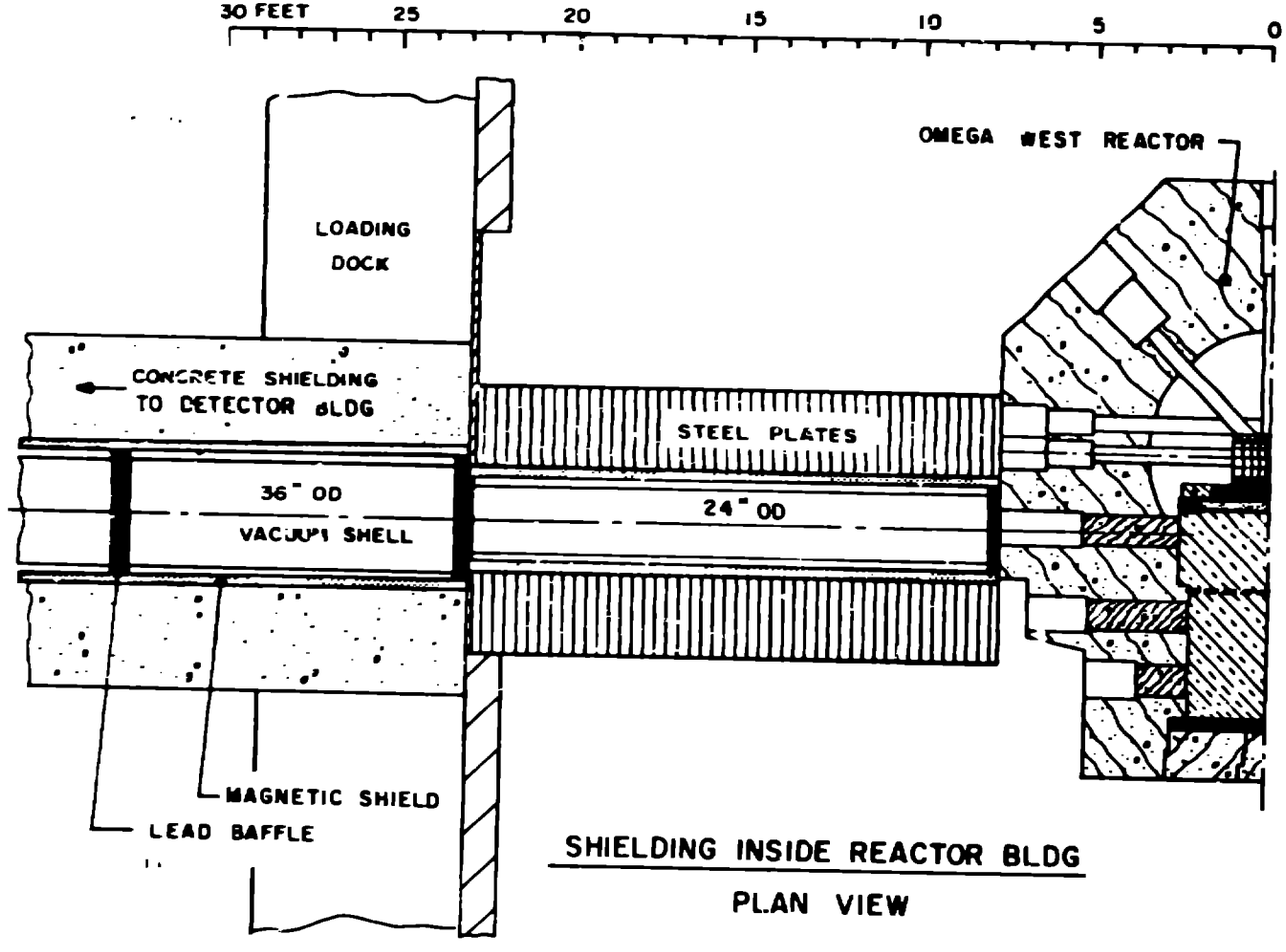

Figure 2. The experiment uses the TG-1S channel at the Omega West Reactor. Graphite stringers in the thermal column close to the core are removed. With tangential extraction the number of fast neutrons and gamma rays from the core at the detector is greatly reduced.

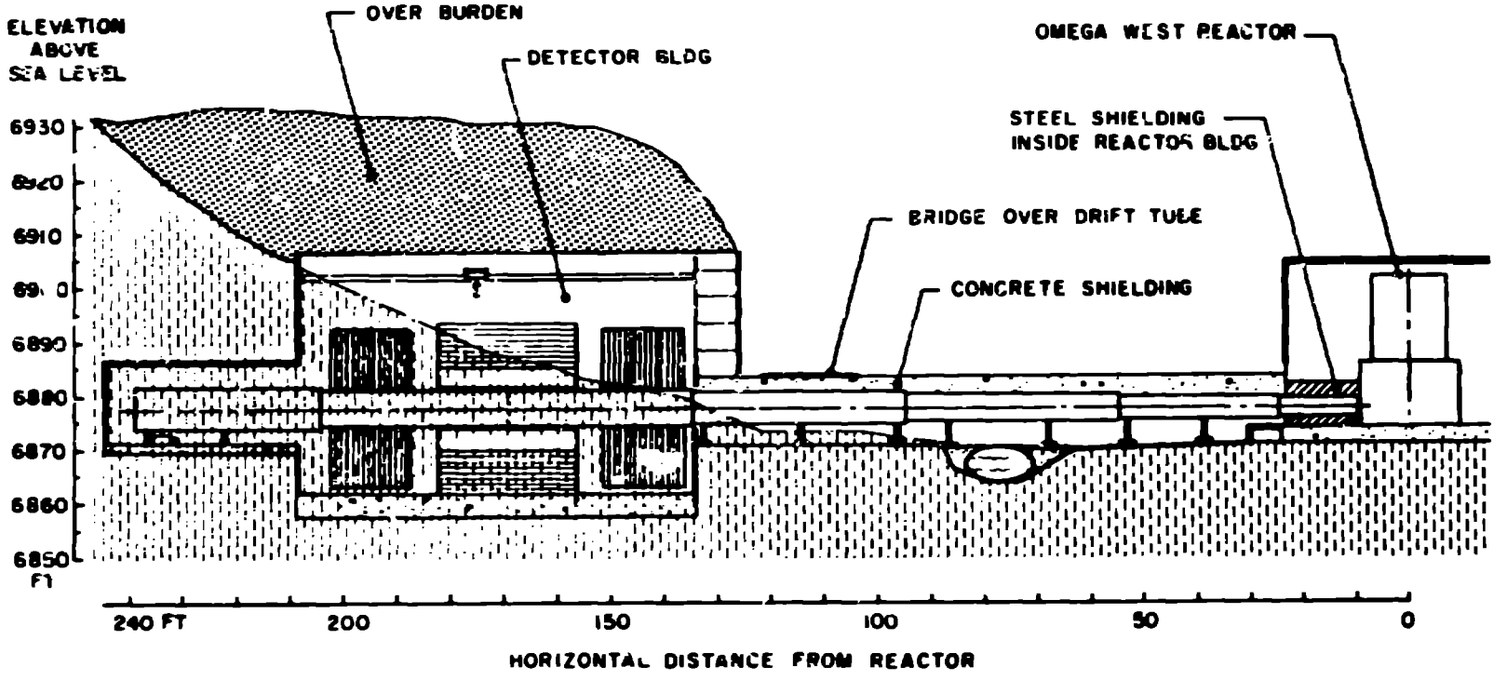

Figure 3. Drift tube and detector building showing detector location and beam stop.

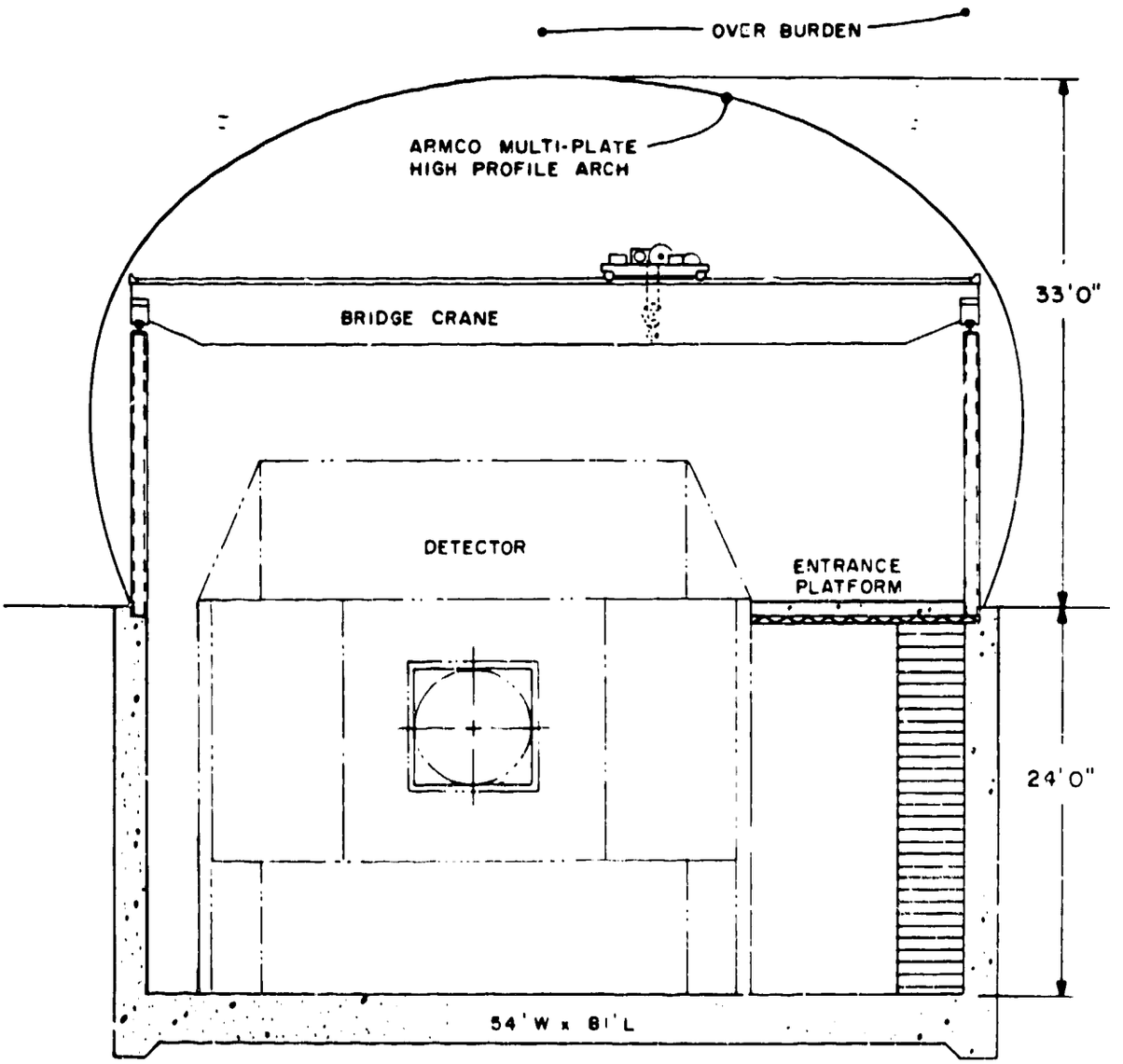

DETECTOR BUILDING
ELEVATION THRU DETECTOR

Figure 4. Elevation view of detector building showing location of drift tube and detector.

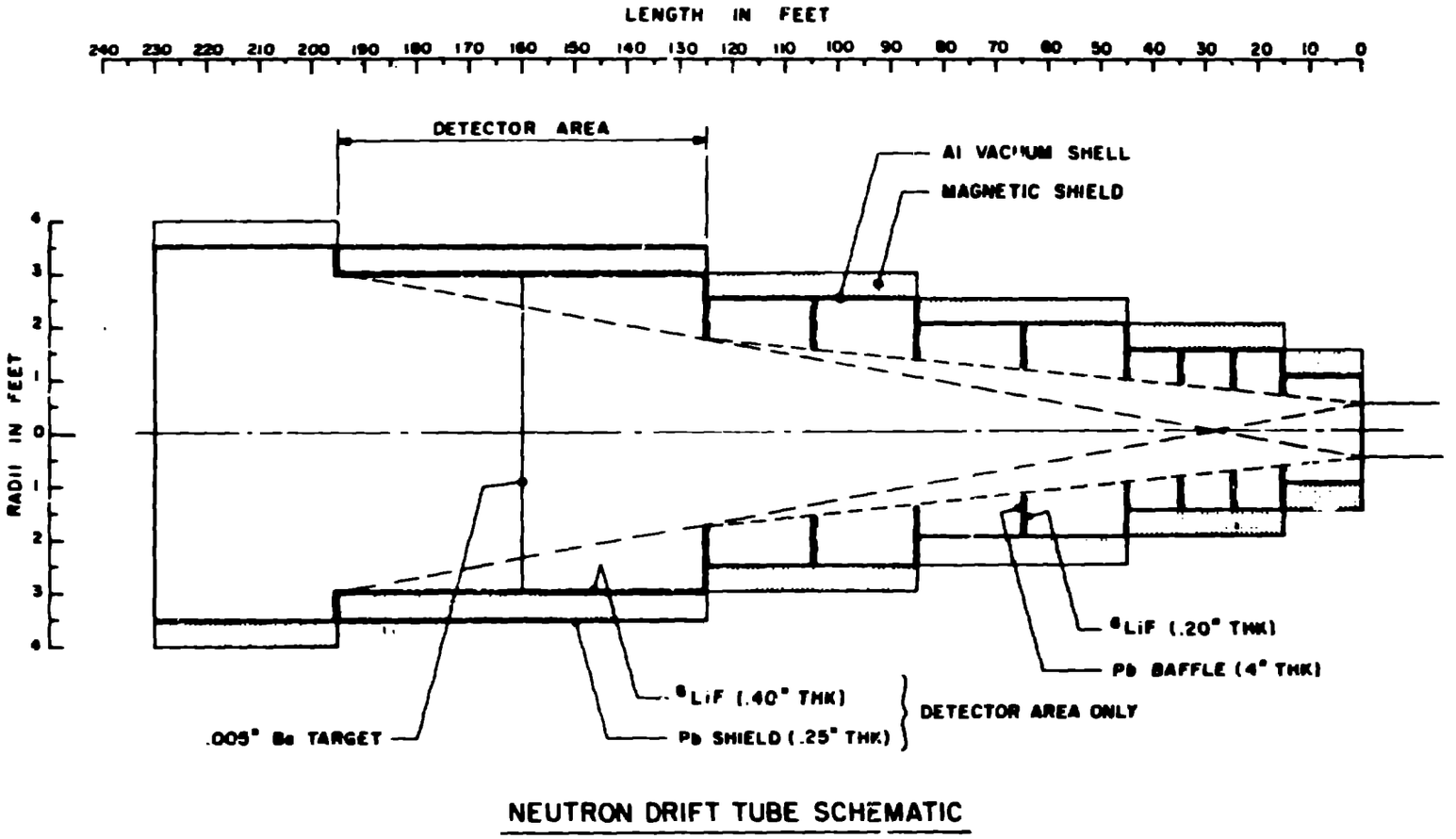

NEUTRON DRIFT TUBE SCHEMATIC

Figure 5. Baffling arrangement along the drift tube. The baffles are lead rings 4 inches thick faced with a layer of ^{6}LiF. The object is to prevent direct neutrons and gammas from the reactor from entering the sensitive regions of the detector.

TABLE I.C.1. PARAMETERS OF THE HOMESTAKE TRACKING SPECTROMETER

Depth:	4850 ft = 1480 m = 4200 meters water equivalent
Cosmic Ray Muon Flux:	1100/m^2/year
Total Mass:	1406 tons (including 90 tons of steel)
Fiducial Mass:	700 tons (averaged over SU(5) decay modes)
Overall Dimensions:	26 ft x 26 ft x 78 ft = 7.9 m x 7.9 m x 23.8 m
Module Dimensions:	26 ft x 1 ft x 1 ft = 7.9 m x 0.3 m x 0.3 m
Number of Modules:	1872 in 3 stacks of crossed layers, 24/layer, 26 layers per stack
Number of Phototubes:	3744
Average Density:	.87 g/cm^3
Radiation Length:	47 cm
Nuclear Absorption Length:	84 cm
Composition (by weight):	74.6 % Carbon 11.0 % Hydrogen 7.0 % Chlorine 6.4 % Iron
Energy Resolution:	10% (FWHM) - electromagnetic 12% (FWHM) - hadronic
Spatial Resolution: (cell size)	30 cm = 54 MeV = 0.64 radiation lengths = 0.36 absorption lengths
Angular Resolution:	4^o (500 MeV electromagnetic cascade, FWHM)
Time Resolution:	3 ns (per module, FWHM)
Vertex Localization Precision:	60 cm (FWHM)
Energy Sensitivity:	8.6 photoelectrons/MeV/module
Usable Detection Threshold:	1.5 MeV (13 photoelectrons)
$\mu \rightarrow e$ Decay Detection Efficiency:	95%
Mean No. of Modules Hit per Event:	
$p \rightarrow e^+\pi^o$	24 }
$p \rightarrow e^+\omega$	15 } = 8000 photoelectrons
$n \rightarrow e^+\pi^-$	17 }

Figure 6. Table I.C.1 from the Homestake Mine Proton Decay Experiment Proposal. The University of Pennsylvania, K. Lande et al., September 1981.

TABLE II.C. LIQUID SCINTILLATOR PROPERTIES

Light output	39% of anthracene
Density (@25° C)	0.84 g/cm^3
H/C Ratio	1.96
Decay time	4 ns
Attenuation length	>8 m
Flash point	300° F
Cost	$4/gal

Figure 7. Table II.C from the Homestake Mine Proton Decay Experiment Proposal.

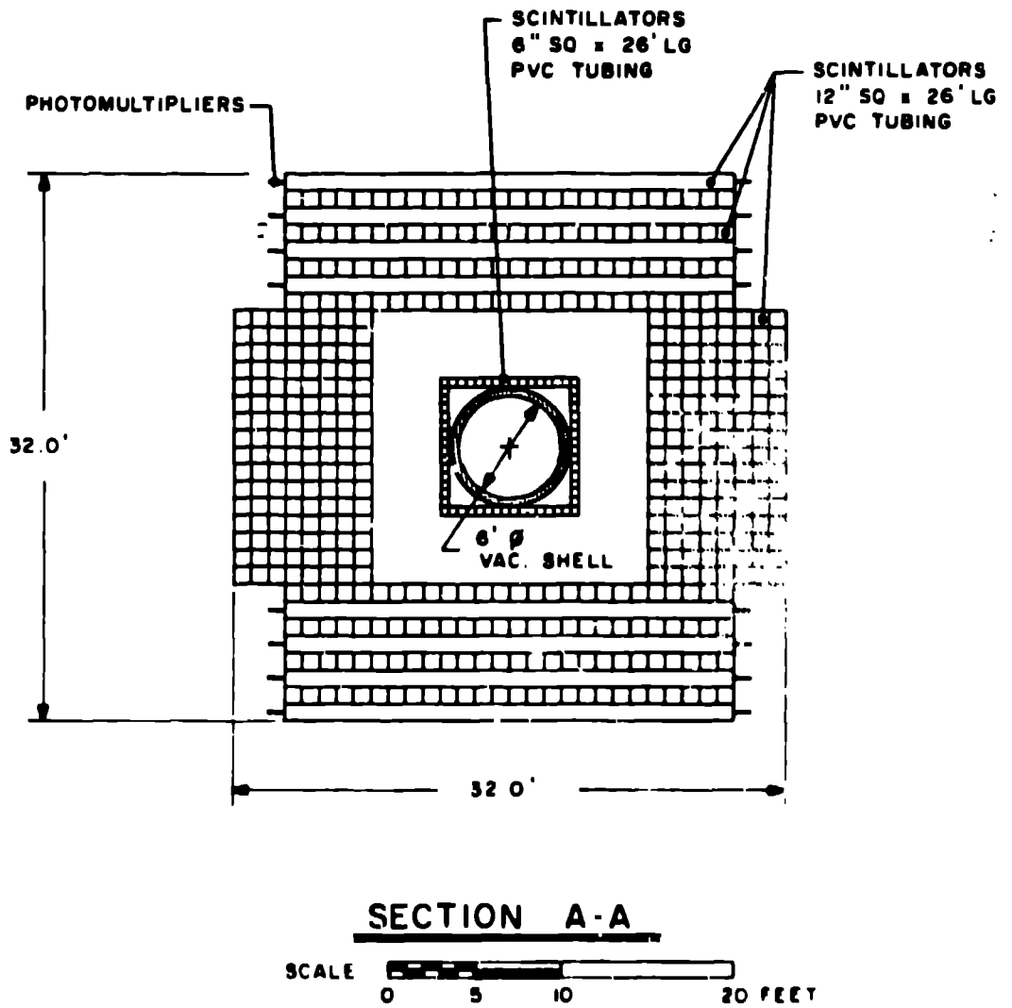

Figure 6. Cross-sectional view of liquid scintillator detector. The time-of-flight gap between the inner and the outer scintillator arrays is 4 feet.

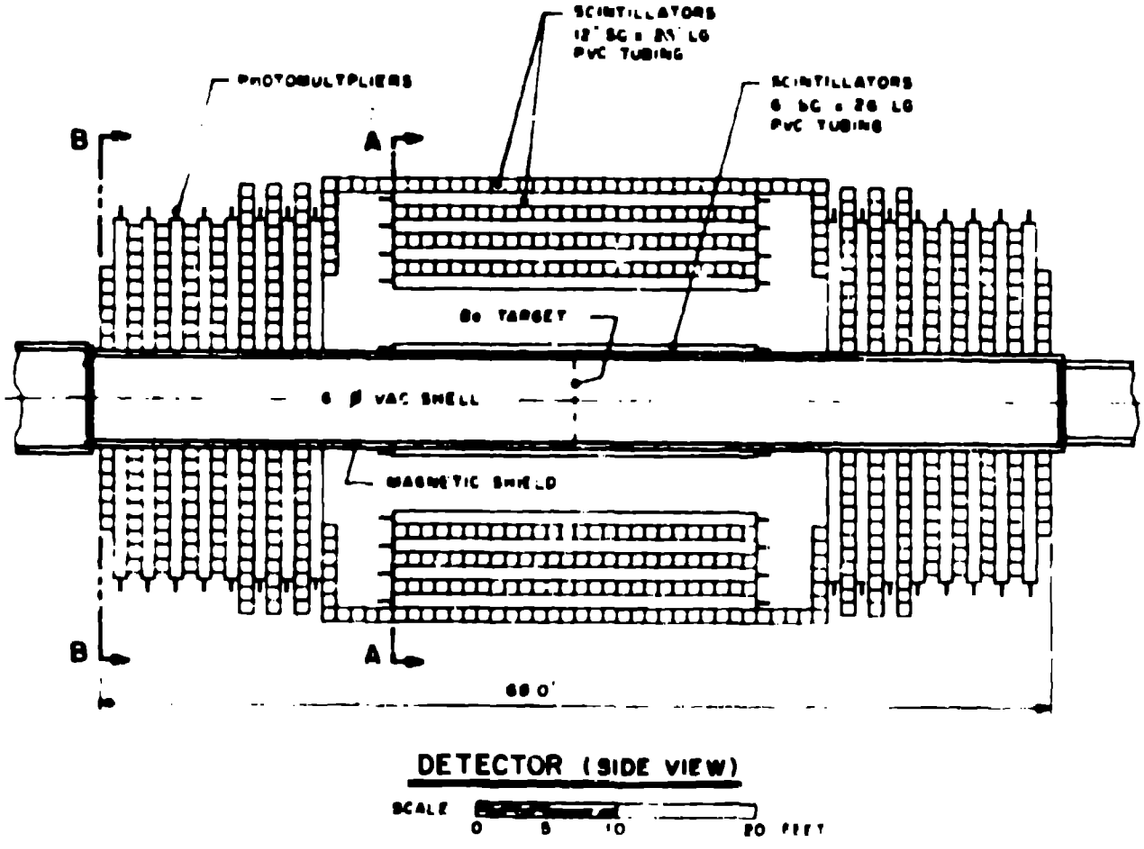

Figure 9. Longitudinal view of liquid scintillator detector with one end sections as shown. The acceptance is 95%. All modules are 26 feet long.

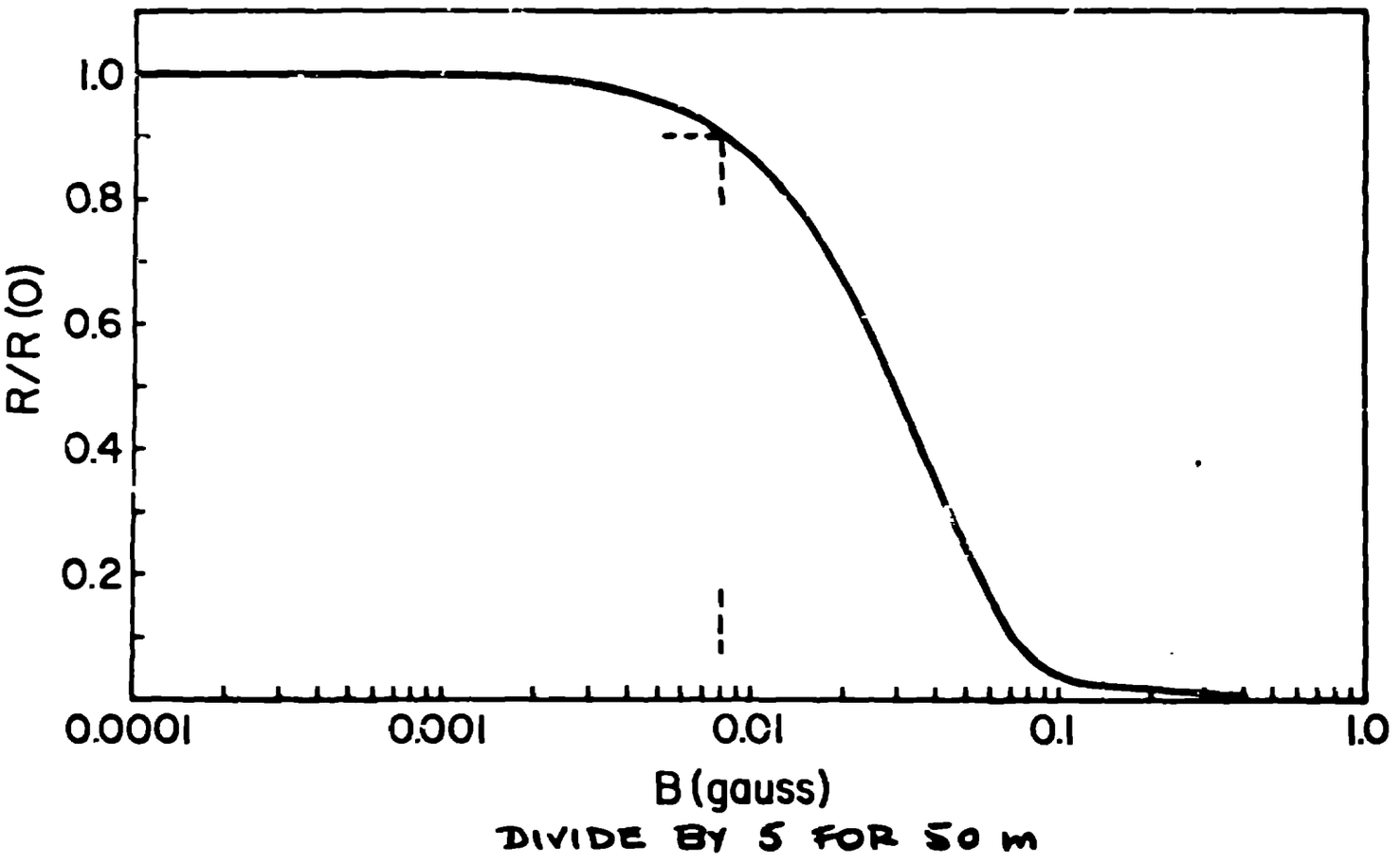

Figure 10. Effect of magnetic field on the conversion rate. The curve is calculated for a Maxwellian distribution of velocities at 400° K and a drift length of 10 m. For 50 m divide B by 5.

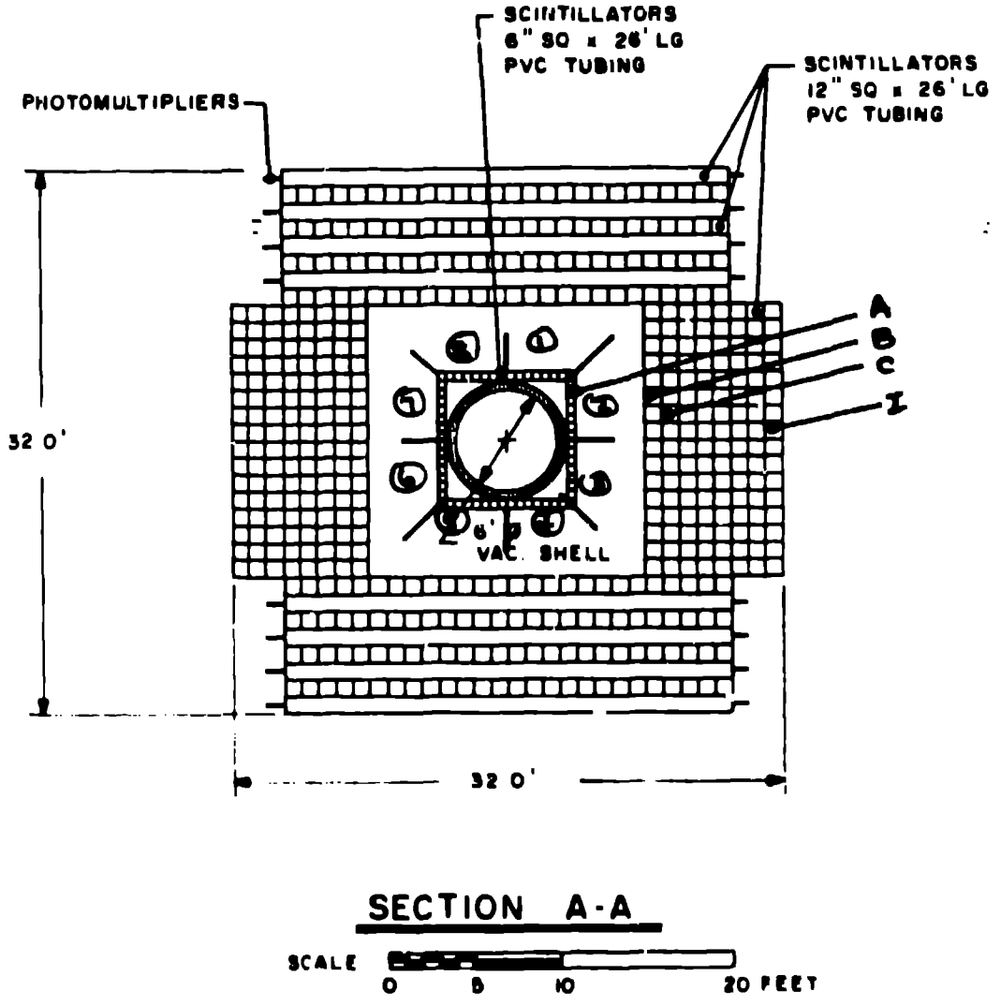

Figure 11. Identification of counter arrays A,B,C,...I. Division of A array into 8 sections.